Electronic Supplementary Material (ESI) for Chemical Communications.

Supporting Information

Structure of the Caffeine·Pyrogallol Complex: Revisiting a Pioneering Structural Analysis of a Model Pharmaceutical Cocrystal

Okba Al Rahal,[a] Michael Ferguson,[a] Cameron B. Lennox,[a, b] Louise Male,[a] Tomislav Friščić[a]

(a) School of Chemistry, University of Birmingham, Edgbaston, Birmingham B15 2TT, United Kingdom.
(b) Department of Chemistry, McGill University, 801 Sherbrooke St. W., Montreal, QC H2L 0B7, Canada.

S1 Computational procedures

S1.1 Structural analysis of the originally proposed caf·pyg·5H$_2$O model

Structural parameters and fractional atomic coordinates for the proposed **caf**·**pyg**·5H$_2$O model[1] were used to construct a structural model that can be viewed by Mercury. Structural analysis of this model revealed several issues, notably the aromatic rings of **pyg** and **caf** being significantly distorted from planarity, one of the water molecules positioned between two hydroxyl groups of **pyg**, and one of the **pyg** C–O bonds sufficiently long to be considered detached from the molecule. Furthermore, the bond lengths and angles of the carbonyl and methyl groups of **caf** were significantly distorted (**Figure S1**). This structural model was validated by periodic DFT as outlined in **S1.2** and **S1.3**.

S1.2 Validation of the proposed caf·pyg·5H$_2$O structural model by DFT and Rietveld refinement

An initial DFT optimisation (see **S1.3** for details of DFT calculations) was attempted, but the errors in the structure were not remediated in the resulting structure. Therefore, we chose to adjust the input structure to ameliorate some of the problems before attempting another optimisation: 1) the fractional *z*-coordinates of the carbon atoms in **pyg** were all set to 0.90, as four of the six carbon atoms were already in such a position; 2) the oxygen atom of the water molecule in close proximity to the -OH groups of **pyg** was shifted by 10% in the crystallographic *z*-direction to remove the overlap; 3) the oxygen and carbon atoms or the carbonyl and methyl group of **caf** were removed and re-inserted using the automatically determined parameters in Mercury[2] program (v2022.3.0). A fixed-cell optimisation was performed and the resulting structure showed no defects or erroneous bonding networks, thus variable-cell optimisation was then performed (**Table S1**). The reported DFT-optimised structure was subjected to geometrically (angle, distance and planar) restrained (**Figure S2**) and geometrically unrestrained Rietveld refinement **Figure S3** using GSAS-i.[3] Rietveld plots for the geometry restrained refinement and R_{wp} and R_p indices (**Table S3**) show that the proposed **caf**·**pyg**·5H$_2$O structure model has significantly poor fit to experimental PXRD data. When no geometry restraints are applied during the refinement, a significant fit improvement (**Table S3**) was achieved; however, this resulted in a structural model that has no chemical sense where the structural integrity of **caf** and **pyg** were completely pulled down.

S1.3 Periodic density-functional theory (DFT) calculations

Periodic DFT calculations were performed using the plane-wave code CASTEP[4] (v22.11), with input files generated using the cif2cell program.[5] On-The-Fly ultrasoft pseudopotentials, obtained from the CASTEP library, were used to describe the core regions of electron density. The exchange-correlation term was described using the PBE[6] functional and the Grimme-D3[7] semi-empirical dispersion correction. The Brillouin zone was sampled using regularly spaced Monkhorst-Pack[8] grids. An initial fixed cell geometry optimisation with a plane wave cut-off energy of 600 eV, ***k***-point spacing of 0.1 2π Å^{-1} was applied. Subsequent optimisations, and optimisations for structural models obtained from single crystal X-ray structure analysis were performed with a plane wave-cut off energy of 800 eV, ***k***-point spacing of 0.06 2π Å^{-1}. The convergence criteria for fixed-cell optimisations were: energy = 1×10^{-3} eV, force = 0.1 eV atom^{-1}, stress = 0.2 GPa, and displacement 5×10^{-3} Å. For variable cell optimisations these tolerances were decreased to: energy = 1×10^{-5} eV, force = 0.03 eV atom^{-1}, stress = 0.05 GPa, and displacement 1×10^{-4} Å.

S1.4 Attempted structure determination from PXRD data

For structural analysis from PXRD data, a high-quality PXRD pattern (see **S2.5**) was indexed using DICVOL.[9] Pawley fit was performed using the reported space group (*P*4/*n*) and the

unit cell parameters obtained from indexing stage. Structure solution was done using DASH.[10-12] For the structure solution step, one optimised structural fragment of **caf** and **pyg** each, and five structural fragments of water molecules from the CSD[13] were imported into DASH. To accelerate structure solution and reduce the number of parameters, hydrogen atoms were omitted, resulting in a total of 27 parameters (six for **caf** and **pyg** each, 15 for water units). A total of 25 simulated annealing structure solution attempts were run, each with a cooling rate of 0.27. The reported pentahydrate structure model[1] and the best three DASH structure solutions (based on intensity χ-squared (Int-χ^2) values, **Table S2**), were selected for further validation *via* periodic DFT optimisation using CASTEP (v22.11), as well as Rietveld refinement[14] using GSAS-i.[3] Periodic DFT validation in all cases showed significant volume expansion (**Table S4**), suggesting that the structural models are not in an energy minimum. Each structural model from DASH was also subjected to Rietveld refinement (**Figures S4-S6**) carried out by the GSAS-i software, with geometric restraints (both bond distance and angle) and planar restraints. In all cases, a significant mismatch as indicated by R indices (**Table S3**) between experimental and calculated PXRD patterns was observed.

S1.5 DFT validation of structures determined by SC-XRD

*Crystal structure of **caf·pyg**·4H₂O*

The disorder of one water molecule in the crystal structure of **caf·pyg**·4H$_2$O (atoms O9 and O9A) leads to two distinct water columns in mutual disorder, based on chains of alternating O−H···O hydrogen bonds of 2.765 Å and 2.773 Å lengths (**Figure S7**). The two chains are identical in structure, but are out of phase with each other by a helix half-turn.

To determine if one chain disorder orientation was preferred over the other, two input configurations were created for DFT optimisation. In the first case, designated as O9A-O9$_0$ (Figure S7 black), both water chains in the system are in-phase with the chains related by an inversion centre in the unit cell In the second case, designated O9A-O9$_\pi$ (Figure S7 blue), the chains are again related by an inversion centre but are out-of-phase with each other by a helix half turn.Optimisation resulted in structures within 1% of the herein experimentally determined structure (**Table S5**), with almost identical cell volumes (%diff = 0.001%). The resulting energies (O9A-O9$_0$ = –1.22550836×10^5, O9A-O9$_\pi$ = –1.22550819×10^5 eV, %diff = 1.4×10^{-5} %), suggest that the water molecule is in a 50:50 disorder regime, indicating equal distribution of the two hydrogen-bonded chain configurations.

*Crystal structure of **caf·pyg***

The crystal structure of **caf·pyg**·4H$_2$O determined by SC-XRD was used without modification for structure optimisation in CASTEP. The resulting structure was in excellent agreement with the experimentally obtained one (**Table S6**).

S1.6 Hydration enthalpy calculation

Using DFT, the hydration enthalpy was calculated using the energy values for **caf·pyg**, **caf·pyg**·4H$_2$O, and an isolated water molecule. The energy of the single water molecule, in a $a = b = c = 30$ Å box was calculated using a fixed cell geometry optimisation using the parameters outlined in **S1.3**, with the exception that only the Γ *k*-point was sampled. The 1×1×2 supercell of the **caf·pyg**·4H$_2$O structure contains 16 pairs of **caf** and **pyg** molecules and 64 water molecules, while the **caf·pyg** structure contains only 4 pairs of **caf** and **pyg** molecules. Therefore, the hydration enthalpy per water molecule was determined as follows:

$$\Delta H_{hyd} = \frac{E_{\mathbf{caf\cdot pyg}\cdot 4\mathrm{H_2O}} - 4E_{\mathbf{caf\cdot pyg}} - 64\,E_{\mathrm{H_2O}}}{64}$$

Where $E_{\mathbf{caf\cdot pyg}\cdot 4\mathrm{H_2O}}$ = –122550.842 eV, $E_{\mathbf{caf\cdot pyg}}$ = –23079.995 eV, and $E_{\mathrm{H_2O}}$ = –471.611 eV. This gives a per water hydration enthalpy of –0.746 eV, or –72.03 kJ·mol^{-1}.

S2 Experimental procedures

S2.1 Synthesis of caf·pyg·4H$_2$O and caf·pyg by ball milling

Samples of **caf·pyg**·4H$_2$O were prepared by ball milling equimolar amounts of **caf** and **pyg** (total weight: 300 mg) in the presence of 75 μL water (η = 0.25 μL mg^{-1}) and 10 mm diameter stainless steel ball. In case of **caf·pyg**, same amount of CH_3NO_2 was used instead of water. Milling was done at a frequency of 30 Hz, for 30 minutes, using a 15 mL volume FTS stainless steel jar mounted on a VWR Beater Mixer Mill.

S2.2 Cocrystal screening by SpeedMixing

In cocrystal screening, an equimolar mixture of **pyg** and **caf** (total scale of 300 mg) was placed in a 12 mL polypropylene cup, placed inside a FlackTek DAC 300 SpeedMixer and spun at 3500 rpm clockwise. Screening parameters included mixing time, liquid additive and η (ratio of liquid additive volume in μL to the total weight of reactants in mg).

S2.3 Solution growth of caf·pyg·4H$_2$O crystals

Crystals of **caf·pyg**·4H$_2$O can be obtained by adding ethyl acetate either to an equimolar mixture of **caf** and **pyg**, or to a **caf·pyg** sample prepared by SpeedMixing, in a 20 mL scintillation vial. In each case, the resulting solution was stirred on a heater set at 50 °C using a magnetic bar (1000 rpm), until a clear solution was obtained. The solution was then covered with a punctured parafilm cover and left to slowly evaporate (for the single crystal used in structure analysis, the laboratory temperature and relative humidity at the start of the crystallisation experiment were 22 °C and 68% RH, respectively, as measured using a digital temperature and relative humidity reader). After two days, rod-shaped crystals were obtained.

S2.4 Solution growth of caf·pyg crystals

Crystals of **caf·pyg** was prepared by stirring (1000 rpm) a sample of either equimolar mixture of **caf** and **pyg**, or of **caf·pyg** prepared by SpeedMixing, with chloroform on a laboratory heater set at 65 °C, followed by addition of acetone to form a clear solution. The solution was then left to slowly evaporate at room temperature, producing block-shaped crystals that were harvested after three days.

S2.5 Powder X-ray diffraction (PXRD)

PXRD data was collected using a Malvern Panalytical Aeris diffractometer operating in reflection mode, with a CuK_α source (λ=1.5406 Å). In a typical experiment, few milligrams of a sample were thinly and uniformly placed on a silicon wafer, and data recorded in 2θ-range 4–50 °, with a step size of 0.017 °. For structure determination attempt, a high-quality PXRD pattern for a **caf·pyg**·4H$_2$O sample prepared by ball milling (see **S2.1**) was recorded using Empyrean Panalytical X-ray diffractometer operating in transmission mode, in the 2θ-range 4–70 °, using a CuK_α source (λ = 1.5406 Å, step size of 0.017°, *ca.* 18 hours).

S2.6 Single crystal X-ray diffraction (SC-XRD)

Single crystal X-ray diffraction measurements were done on an Agilent SuperNova Dual Atlas diffractometer equipped with a mirror monochromator and CuK_α (λ = 1.5418 Å) radiation. Crystal temperature was controlled using an Oxford Cryosystems thermostat. Structure solution and refinement were carried out using SHELXT[15] and SHELXL.[16] Refinement of non-hydrogen atoms was carried out using an anisotropic model, and some of the hydrogen atoms (attached to hydroxy groups of **pyg**) were located in the electron density and freely refined while the rest of hydrogen atoms were inserted in idealized positions, and included in refinement following a riding model, with U_{iso} set at 1.2 times the U_{eq} value of the associated carbon atom.

S2.7 Simultaneous thermogravimetric analysis and differential scanning calorimetry (TGA/DSC)

Simultaneous DSC-TGA measurements were carried out using a STD 650 TA instrument. Approximately 25 mg of the sample was added into an open alumina pan which was then placed inside the cell of the instrument. An empty open alumina pan was used as a DSC reference. The sample was heated from room temperature up to 350 °C at a heating rate of 0.5 °C/min, under a dynamic atmosphere of nitrogen gas (50 mL/min).

S2.8 Fourier-transform infrared attenuated total reflectance (FTIR-ATR) spectroscopy

FTIR-ATR spectra were recorded using a Spectrum Two (UATR) PerkinElmer instrument, with each spectrum measured by taking the average of 16 scans in the range 4000 – 450 cm^{-1}.

S2.9 Dynamic vapour sorption (DVS)

DVS analysis was carried out using DVS Resolution instrument (Surface Measurement System). Approximately 20 mg of sample was put in an aluminium pan, which was then placed inside the DVS chamber. Mass change was recorded as a function of relative humidity (RH) at a constant temperature (25 °C). One cycle of sorption-desorption starting from 0% RH up to 90% RH at an increment of 10% RH was carried out.

S2.10 Variable-temperature PXRD (VT-PXRD) analysis

VT-PXRD analysis was carried out by heating up a **caf·pyg**·$4H_2O$ sample from 20 °C up to 100 °C, at a heating rate of 10 °C/min using an Anton Paar HTK 1200 N unit attached to a D8 Advance (Bruker) diffractometer. At each interval, data collection time was 10 minutes, with the temperature held constant during data collection.

S2.11 Hot-stage microscopy (HSM)

HSM Thermal microscopy was performed with a LINKAM LNP96-S temperature-controlled stage and recorded using a Allied vision Alvium 1800 U-1240c camera mounted on a Leica DM2500 LED microscope using a 10x objective. All videos and pictures in Figures SX) include a scale bar (125 mm) and are white balance corrected. A few milligrams of **caf·pyg**·$4H_2O$ were dispersed on a glass slide which was then placed inside the hot stage linked to a temperature control unit. Videos were recorded while the sample was heated from ambient temperature up to 140 °C, at a rate 1 °C/min.

S3 Results

S3.1 Structural analysis of proposed caf·pyg·$5H_2O$ structural model

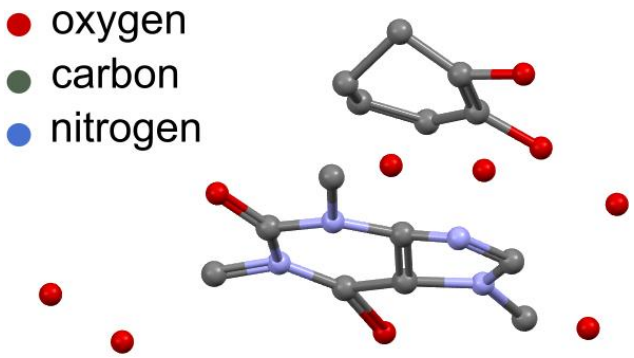

Figure S1. Asymmetric unit contents for the structural model of the solid-state complex constructed from atomic coordinates reported by Arnone and Marchessault.[1]

S3.2 Validation of caf·pyg·5H$_2$O structural model by DFT and Rietveld refinement

Table S1. Comparison of cell parameters for the proposed **caf**·**pyg**·5H$_2$O structure model before and after periodic DFT optimisation.

Unitcell parameter	**caf**·**pyg**·5H$_2$O structure model		Difference (%)
	before DFT	after DFT	
a / Å	23.26	25.00655	7.51
b / Å	23.26	25.00655	7.51
c / Å	6.99	6.98547	-0.06
V / Å^3	3781.78	4367.64	15.49

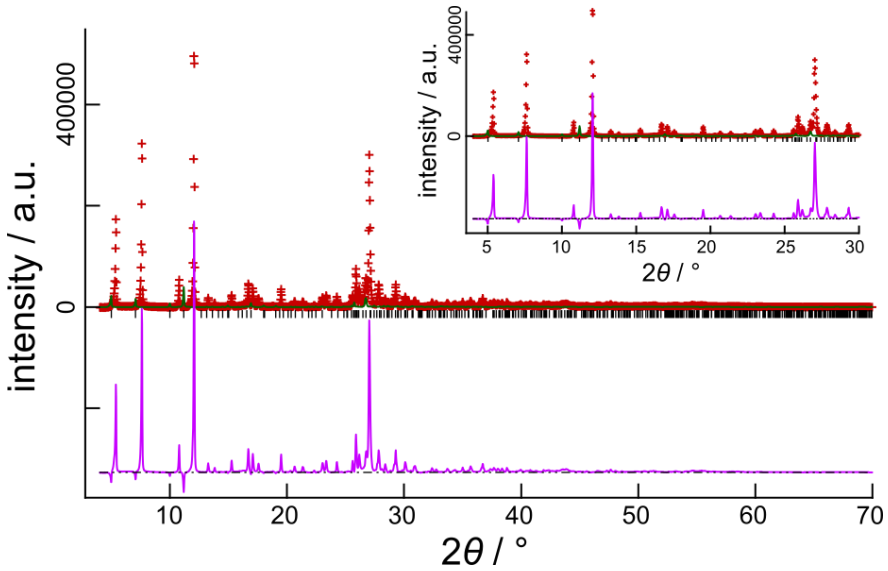

Figure S2. Geometry restrained Rietveld refinement plot for the reported DFT-optimised structure with geometrical restraints. Red crosses = experimental PXRD pattern after background subtraction, green line = calculated pattern, black tick marks = predicted peak positions, magenta line = difference plot.

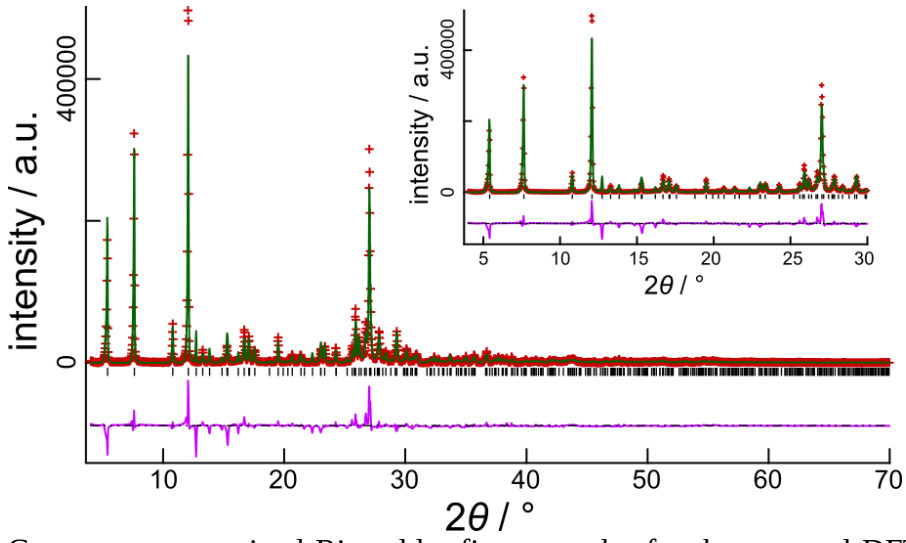

Figure S3. Geometry unrestrained Rietveld refinement plot for the reported DFT-optimised structure but without geometrical restraints. Red crosses = experimental PXRD pattern after background subtraction, green line = calculated pattern, black tick marks = predicted peak positions, magenta line = difference plot.

S3.3 Attempted structure solution from PXRD data

Table S2. Summary Int-χ^2 values for best three solutions obtained from DASH.

Solution #	Int-χ^2
1	14.25
2	14.83
3	14.91

Table S3. Summary of the *R*-values for the Rietveld refinement fitting of the reported DFT optimised structure and the structures obtained by DASH.

Structural model	R_{wp} (%)	R_p (%)
Reported DFT optimised (geometrically restrained refinement)	46.54	33.74
Reported DFT optimised (geometrically unrestrained refinement)[a]	13.36	8.06
DASH solution 1	16.11	11.43
DASH solution 2	17.73	12.57
DASH solution 3	20.50	14.32

[a)]structural model broke down.

Table S4. Comparison of cell parameters for the experimental indexing (Exp) with the three structural models obtained by DASH after DFT optimisation.

Unitcell parameter	Exp	DASH solution after DFT[a] 1	2	3
a / Å	23.16506 (0.00403)	23.92542 (3.3%)	24.44539 (5.5%)	25.26607 (9.1%)
b / Å	23.16506 (0.00403)	23.92542 (3.3%)	24.44539 (5.5%)	25.26607 (9.1%)
c / Å	6.94431(0.00199)	6.96957 (0.4%)	6.78011 (-2.4%)	8.26289 (19.0%)
V / Å^3	3726.46	3989.56 (7.1%)	4051.64 (8.7%)	5274.82 (41.55%)

a) Values in parentheses are the percentage difference relative to the experimental unit cell determined by PXRD.

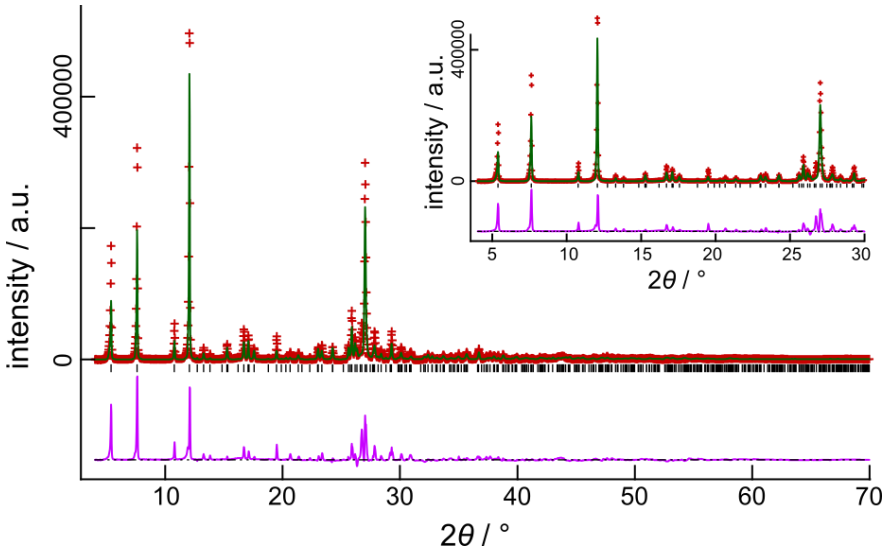

Figure S4. Rietveld refinement plot for DASH solution 1. Red crosses: experimental PXRD pattern after background subtraction, green line: calculated pattern, black tick marks: predicted peak positions, magenta line: difference plot.

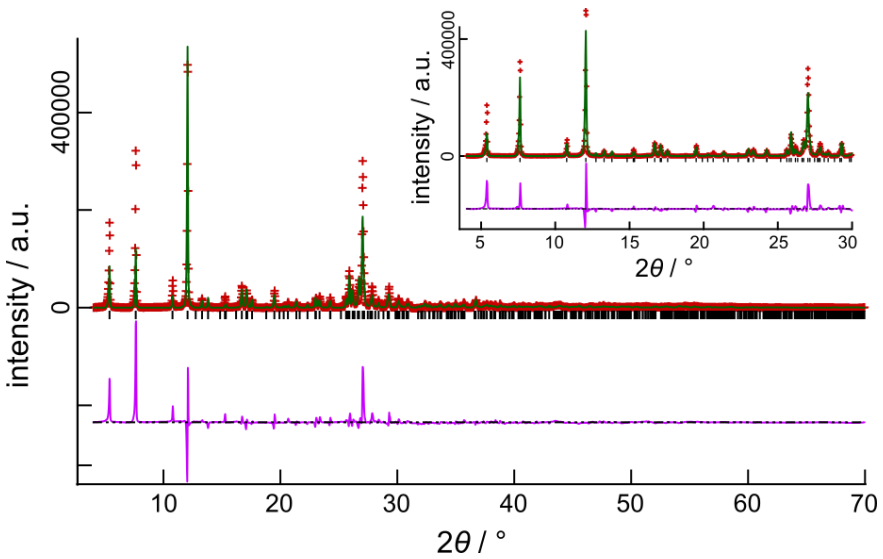

Figure S5. Rietveld refinement plot for DASH solution 2. Red crosses: experimental PXRD pattern after background subtraction, green line: calculated pattern, black tick marks: predicted peak positions, magenta line: difference plot.

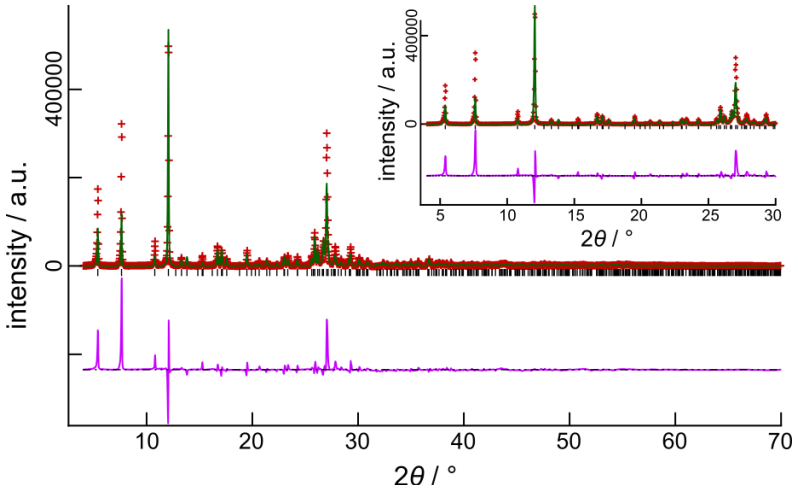

Figure S6. Rietveld refinement plot for DASH solution 3. Red crosses: experimental PXRD pattern after background subtraction, green line: calculated pattern, black tick marks: predicted peak positions, magenta line: difference plot.

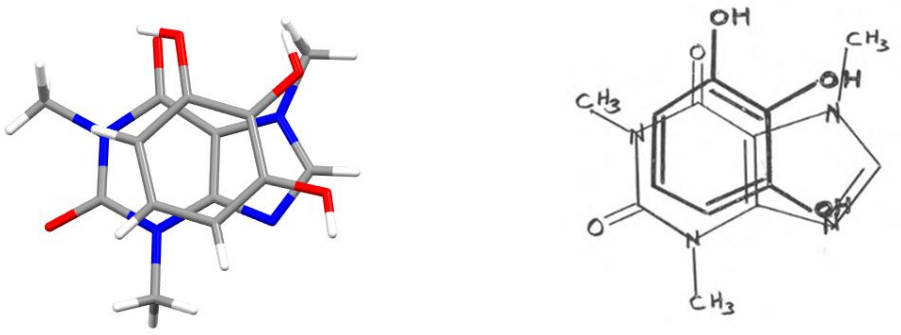

Figure S7. Comparison of: (left) the π-stacked arrangement of a pair of **caf** and **pyg** molecules in the crystal structure of **caf**·**pyg**·4H_2O to (right) the proposed arrangement in the **caf**·**pyg**·5H_2O model.[17]

S3.4 DFT and Rietveld validation of structures determined by SC-XRD

Crystal structure of caf·pyg·4H$_2$O

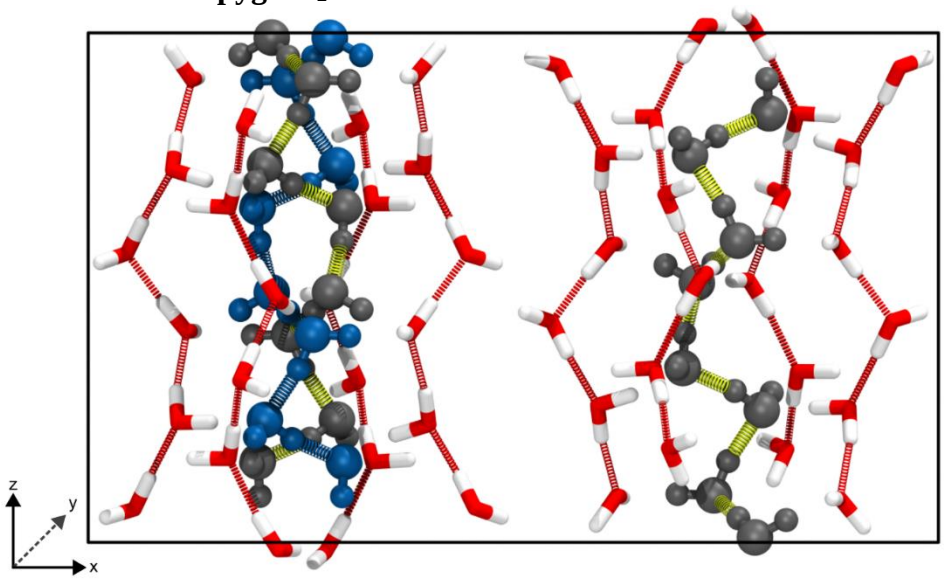

Figure S8. Image of the disordered water chains in the two water columns within a 1×1×2 supercell of the **caf·pyg**·4H$_2$O structure. For DFT validation of the relative occupancies of O9 and O9A atoms (and, accordingly the relative occupancies of the two disordered chain configurations), two structural models were optimised and energies compared using CASTEP. In each model, one chain (right, black) was uniquely defined, while the other one was set to adopt one of two possible disordered arrangements (shown in black and blue) mutually related by a helix half-turn.

Table S5. Comparison of cell parameters for a 1×1×2 supercell of the **caf·pyg**·4H$_2$O structure measured by SC-XRD with the two chain models optimised using CASTEP to determine the preferred arrangement of the disordered water molecule (O9 or O9A).

Cell parameter	SCXRD (1×1×2)	O9A-O9$_0$	O9A-O9$_\pi$
a / Å	23.1123	22.95888 (-0.66 %)	22.94612 (-0.72%)
b / Å	23.1123	22.95888 (-0.66 %)	22.94612 (-0.72 %)
c / Å	13.6898	13.75056 (0.44 %)	13.75248 (0.46 %)
V / Å^3	7312.80	7248.09 (-0.88%)	7241.02 (-0.98%)

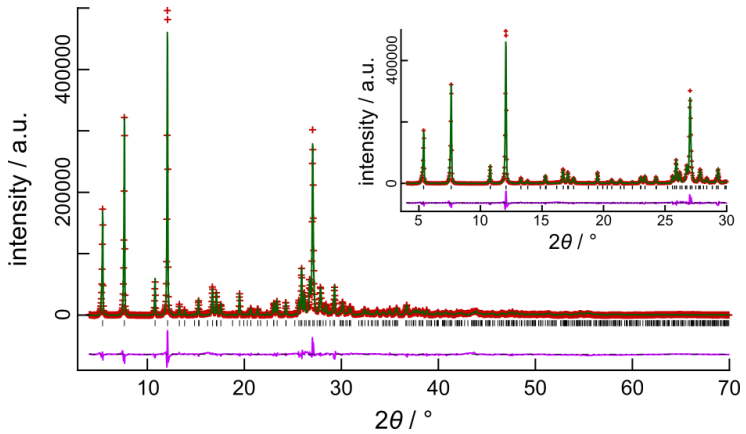

Figure S9. Rietveld refinement plot for **caf·pyg**·4H$_2$O structure obtained by SC-XRD. Red crosses: experimental PXRD pattern after background subtraction, green line: calculated pattern, black tick marks: predicted peak positions, magenta line: difference plot.

Crystal structure of caf·pyg

Table S6. Comparison of crystallographic unitcell parameters for the **caf·pyg** structure obtained from single crystal X-ray diffraction before and after DFT optimisation.

Cell parameter	experiment	DFT	Difference (%)
a / Å	13.878(1)	13.83617	-0.30
b / Å	7.5913(4)	7.70399	1.48
c / Å	15.015(1)	15.00454	-0.07
V / Å^3	1410.16(2)	1422.46	0.87

S3.5 Cocrystal screening by SpeedMixing

Table S7. Summary of cocrystal screening experiments based on SpeedMixing. In rows 29, reactants were sieved through a 200 μm sieve prior to reaction. All experiments were done at 3500 rpm, using 12 mL polypropylene cups, and conversion was evaluated by PXRD.

	Liquid	**η (μL mg^{-1})**	**Mixing time (min)**	**Total scale (mg)**	**Full conversion**
1	acetonitrile	0.62	5	320	No
2	acetonitrile	0.62	10	320	No
3	methanol	0.62	5	320	No
4	methanol	0.62	10	320	No
5	acetone	0.62	10	320	No
6	acetone	0.62	15	320	No
7	chloroform	0.31	20	320	No
8	chloroform	0.62	5	320	No
9	chloroform	0.62	10	320	No
10	o-xylene	0.62	5	320	No
11	o-xylene	0.62	10	320	No
12	ethyl acetate	0.62	5	320	No
13	ethyl acetate	0.62	10	320	No
14	ethyl acetate	0.62	15	320	No
15	nitromethane	0.62	5	320	No
16	nitromethane	0.1	10	300	No
17	nitromethane	0.2	10	300	No
18	nitromethane	0.3	10	300	No
19	nitromethane	0.3	15	300	No
20	nitromethane	0.4	15	300	No
21	nitromethane	0.4	20	300	No
22	nitromethane	0.4	25	300	No
23	nitromethane	0.4	30	300	No
24	nitromethane	0.4	35	300	No
25	nitromethane	0.5	5	300	No
26	nitromethane	0.5	10	300	No
27	nitromethane	0.5	15	300	No
28	nitromethane	0.5	20	300	No
29	nitromethane	0.4	10	300	Yes (**caf·pyg**)
30	water	0.3	5	300	Yes (**caf·pyg**·4H_2O)

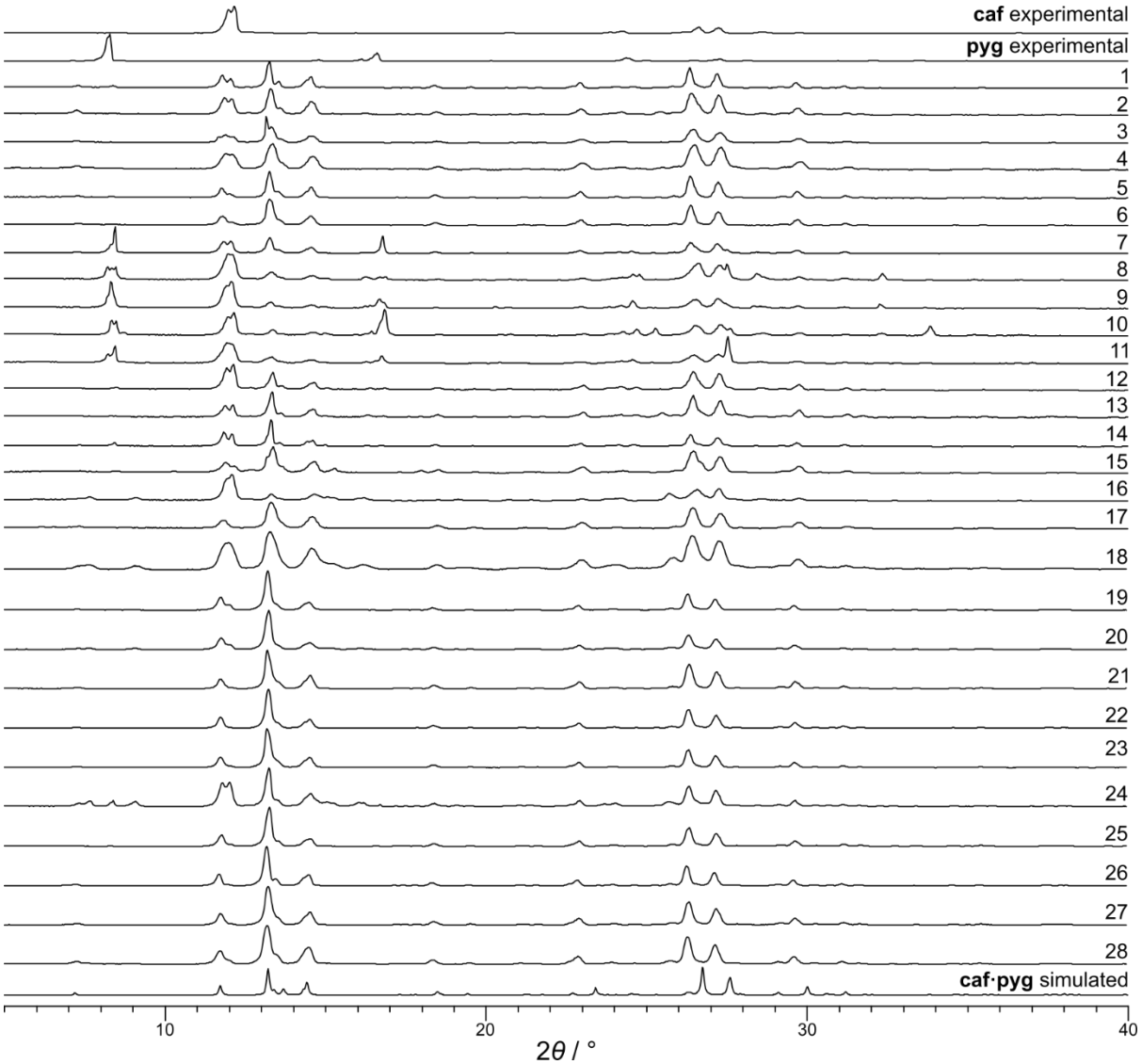

Figure S10. Experimental PXRD patterns for SpeedMixing cocrystal screening experiments that gave partial conversion to **caf·pyg** (**Table S7**).

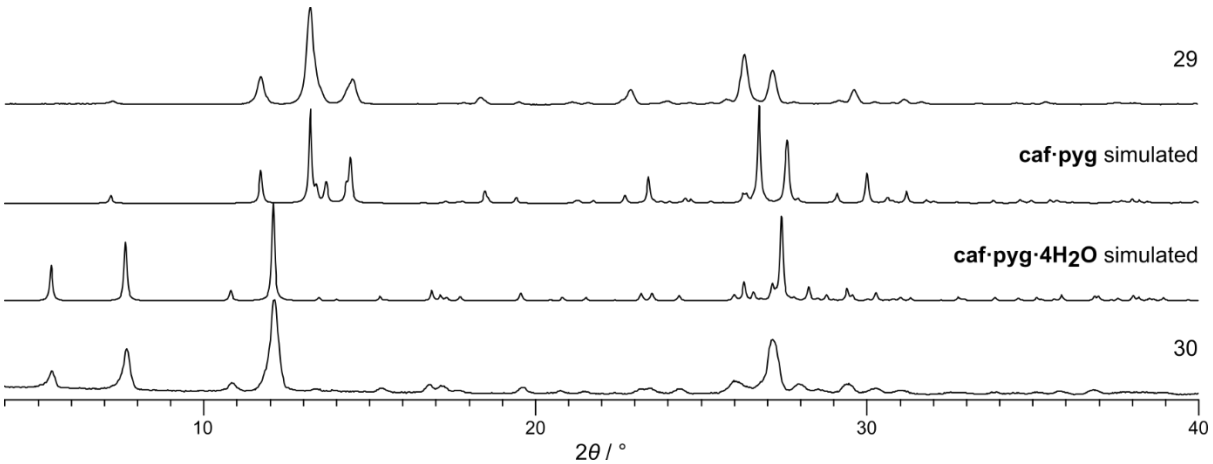

Figure S11. Experimental PXRD patterns for cocrystal screening experiments that gave full conversion into **caf·pyg** or **caf·pyg**·4H_2O (**Table S7**).

S3.6 Hydration/dehydration study

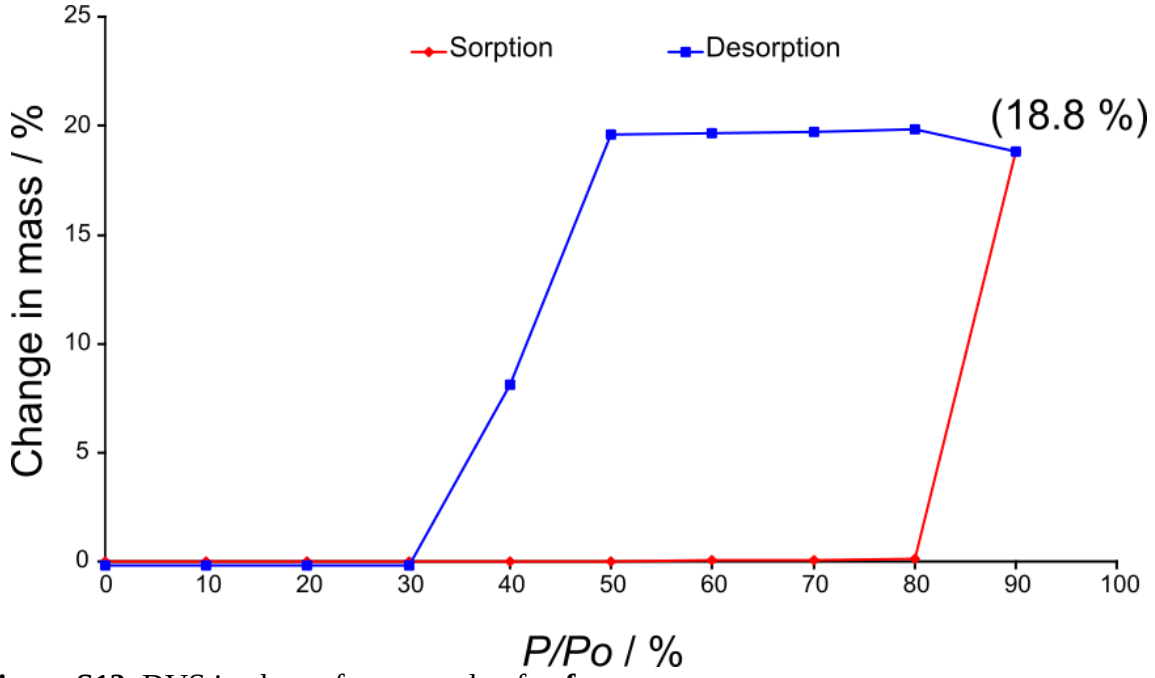

Figure S12. DVS isotherm for a sample of **caf·pyg**.

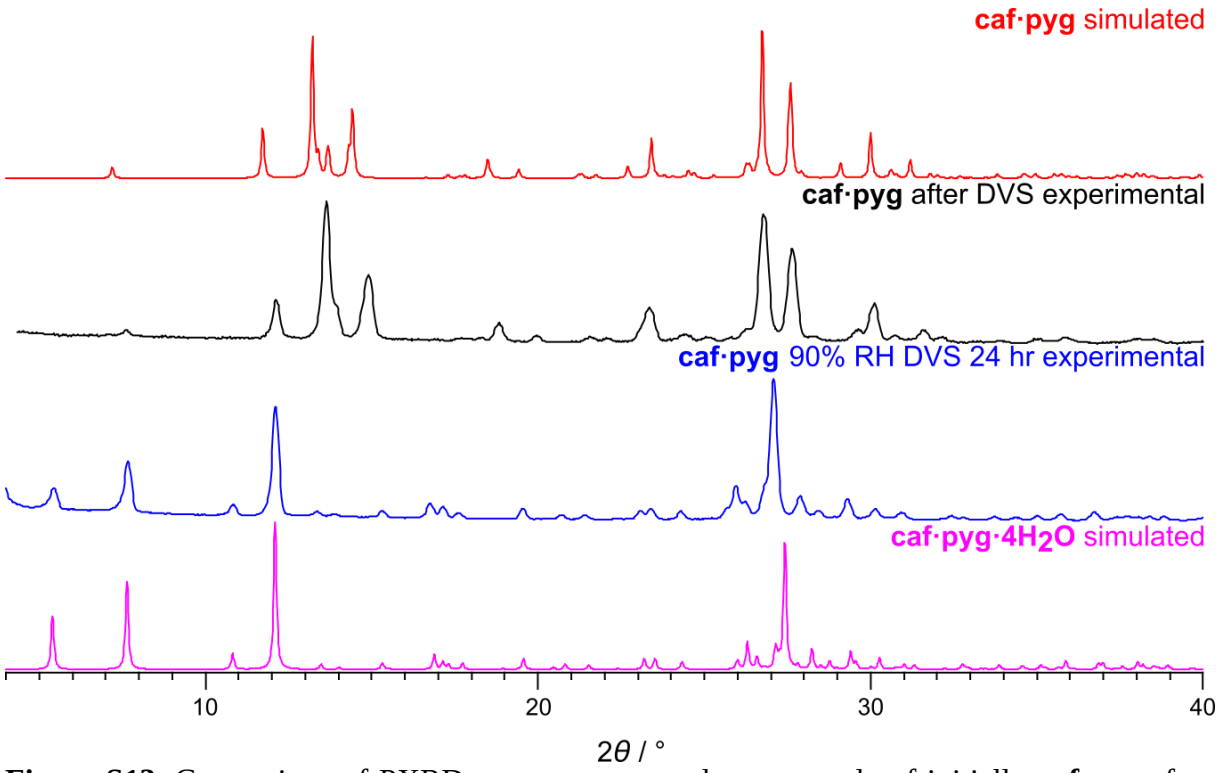

Figure S13. Comparison of PXRD patterns measured on a sample of initially **caf·pyg** after one adsorption and desorption cycle in the DVS (Figure S11), and also after being held at 90% RH in the DVS balance over 24 hours.

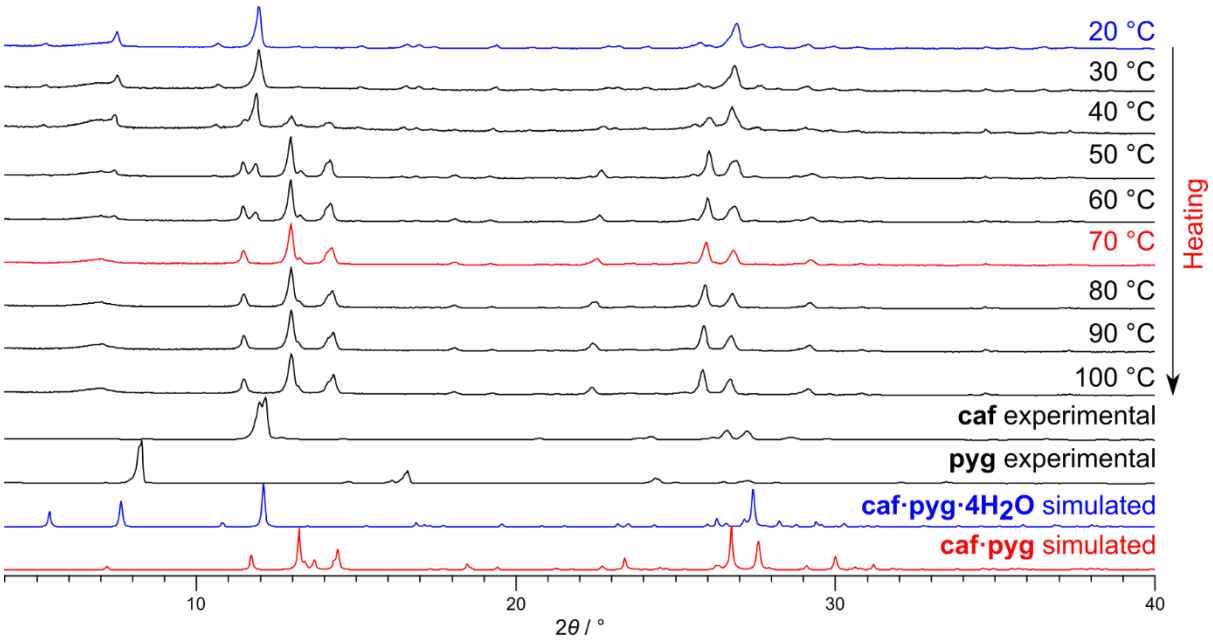

Figure S14. Comparison of PXRD patterns from a variable temperature **caf·pyg**·4H_2O dehydration experiment.

S3.7 Physical mixture aging study

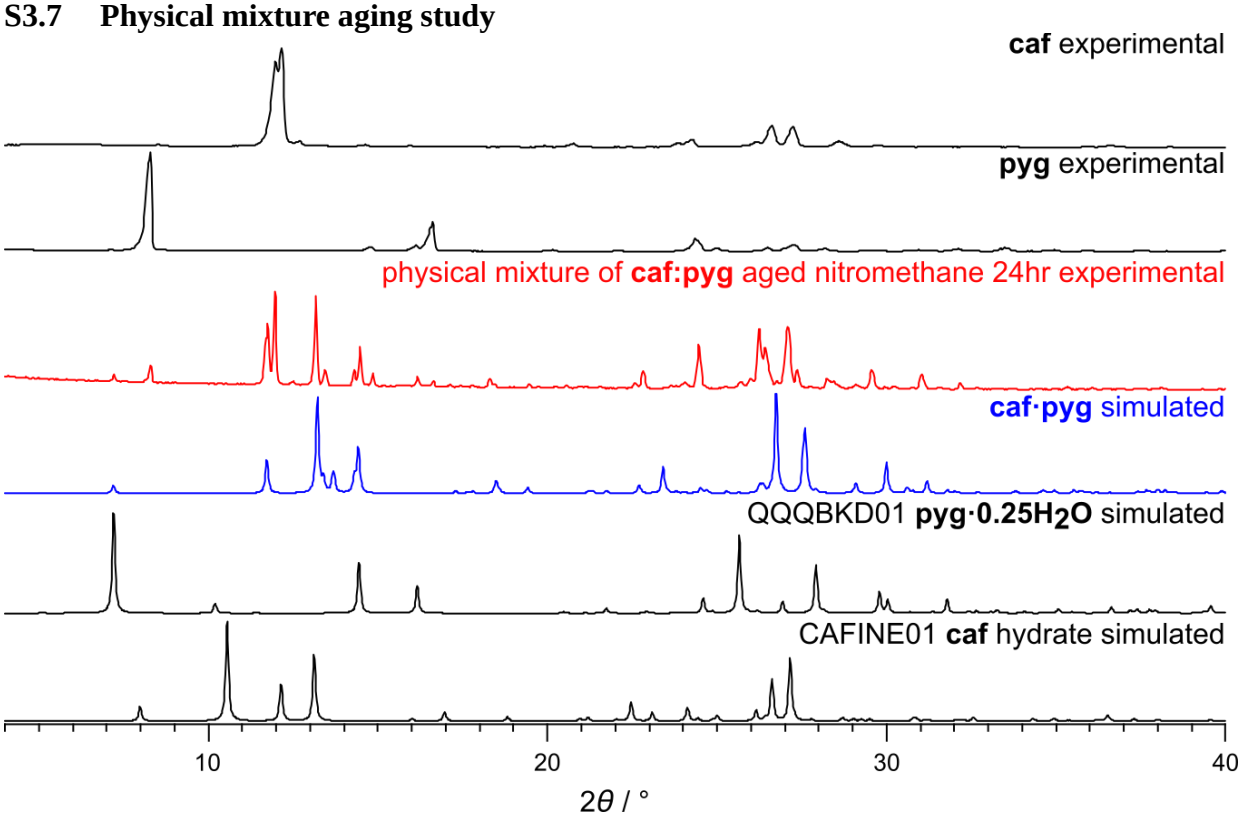

Figure S15. Comparison of PXRD patterns for ageing of a 1:1 stoichiometric mixture of **caf** and **pyg** in nitromethane vapour (from top to bottom): commercial **caf**; commerical **pyg**; sample after 24 hours ageing and simulated PXRD patterns for structures of **caf·pyg**, **pyg**·0.25H_2O and **caf** hydrate.

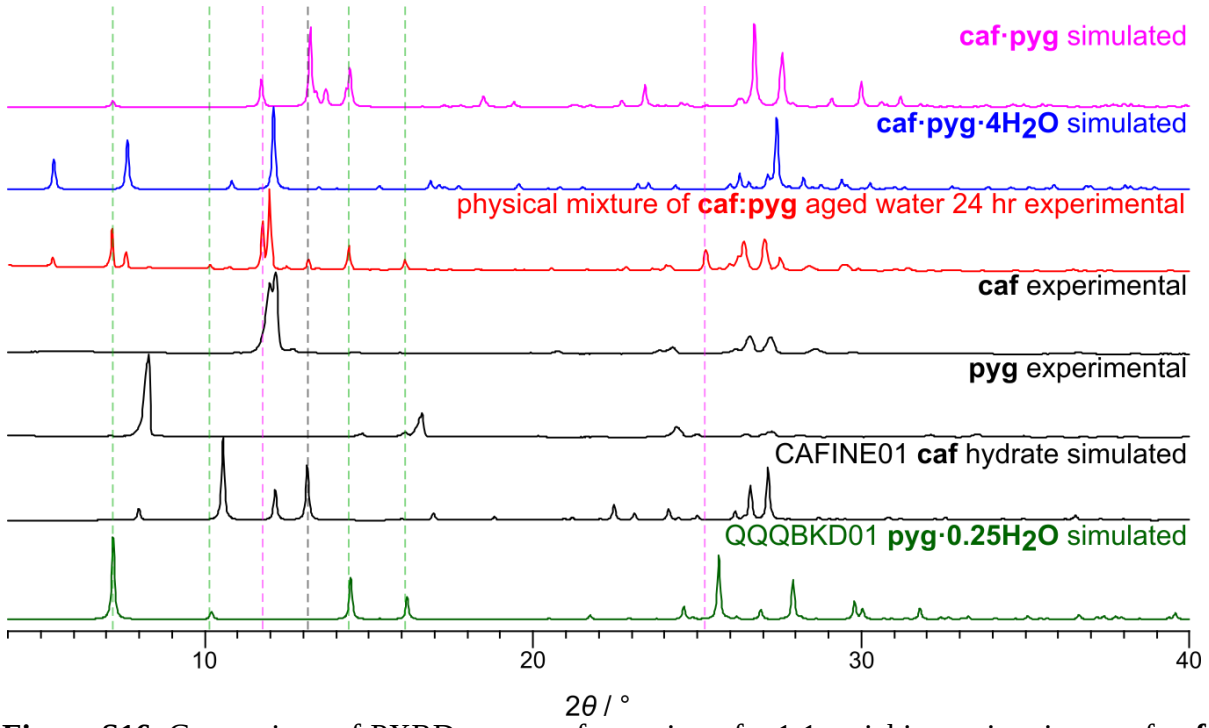

Figure S16. Comparison of PXRD patterns for ageing of a 1:1 stoichiometric mixture of **caf** and **pyg** in 100% RH (from top to bottom): simulated for crystal structures of **caf·pyg** and **caf·pyg**·4H_2O; measured for the sample after 24 hours ageing; commercial **caf**; commercial **pyg**, and simulated for structures of **caf** hydrate and **pyg**·0.25H_2O.

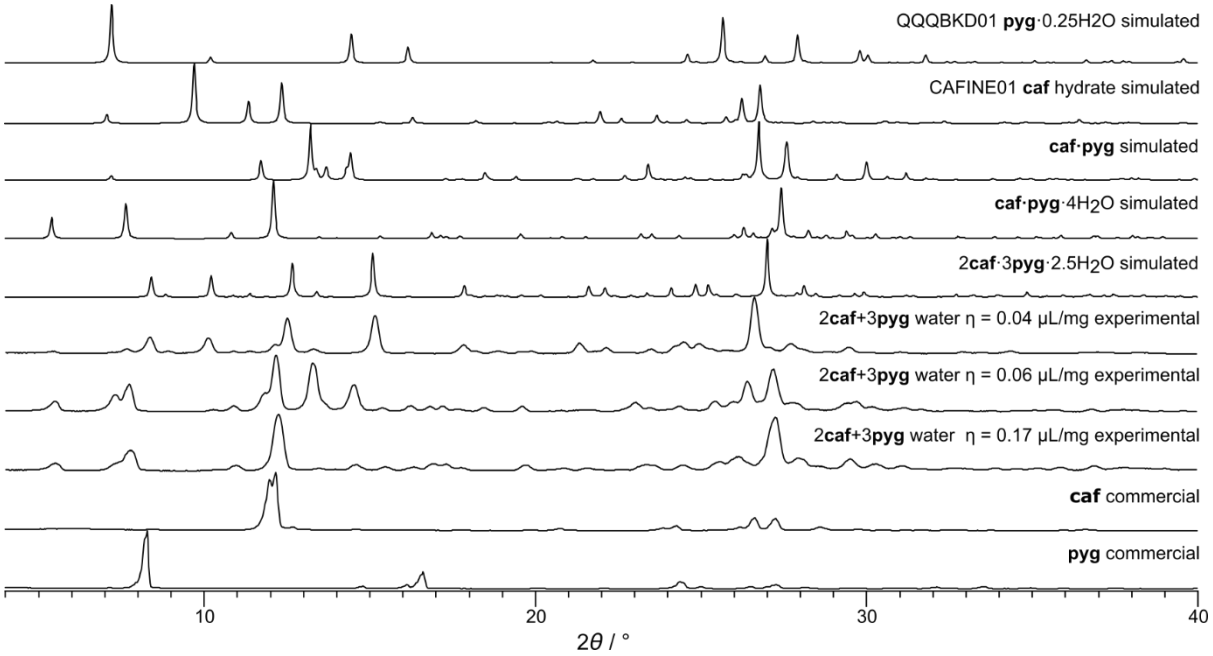

Figure S17. Comparison of PXRD patterns for ball milling reaction involving caf and pyg in respective 2:3 stoichiometric ratio, in the presence of water additive (from top to bottom): simulated for crystal structures of **pyg**·0.25H_2O; **caf** hydrate; **caf·pyg**; **caf·pyg**·4H_2O and **2caf·3pyg**·2.5H_2O; measured for reactions at η = 0.04 μL/mg; 0.06 μL/mg and 0.17 μL/mg; commercial **caf** and commercial **pyg**.

S3.8 Thermal analysis (TGA/DSC and HSM)

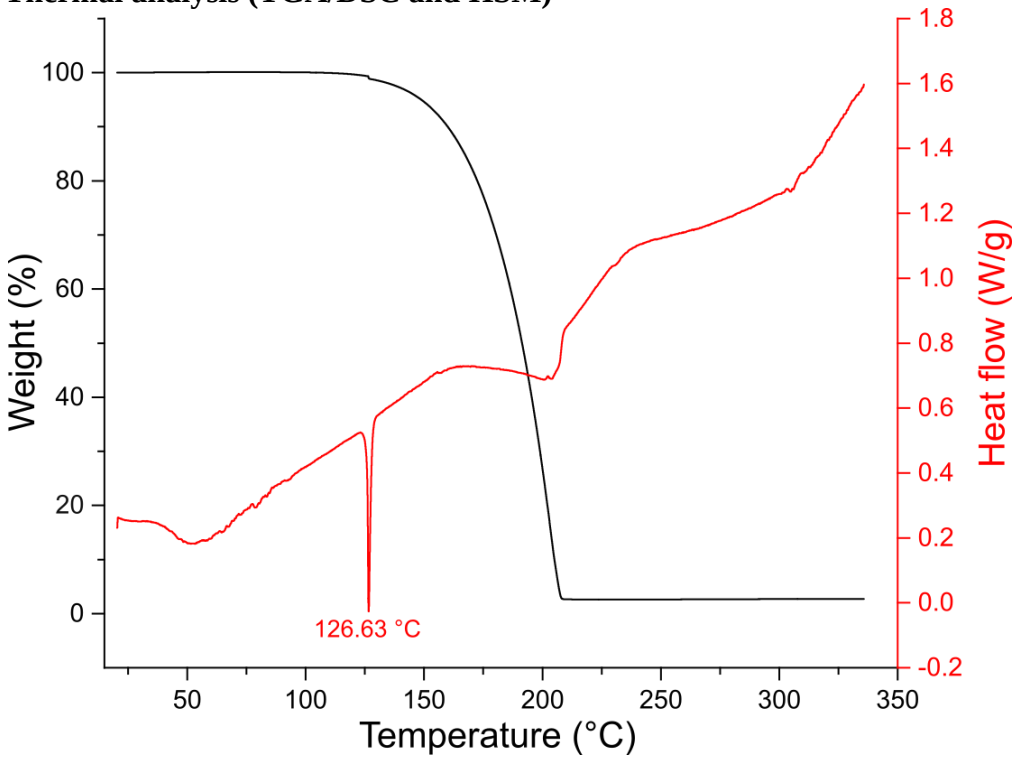

Figure S18. Simultaneous DSC-TGA thermogram for the **caf·pyg** cocrystal.

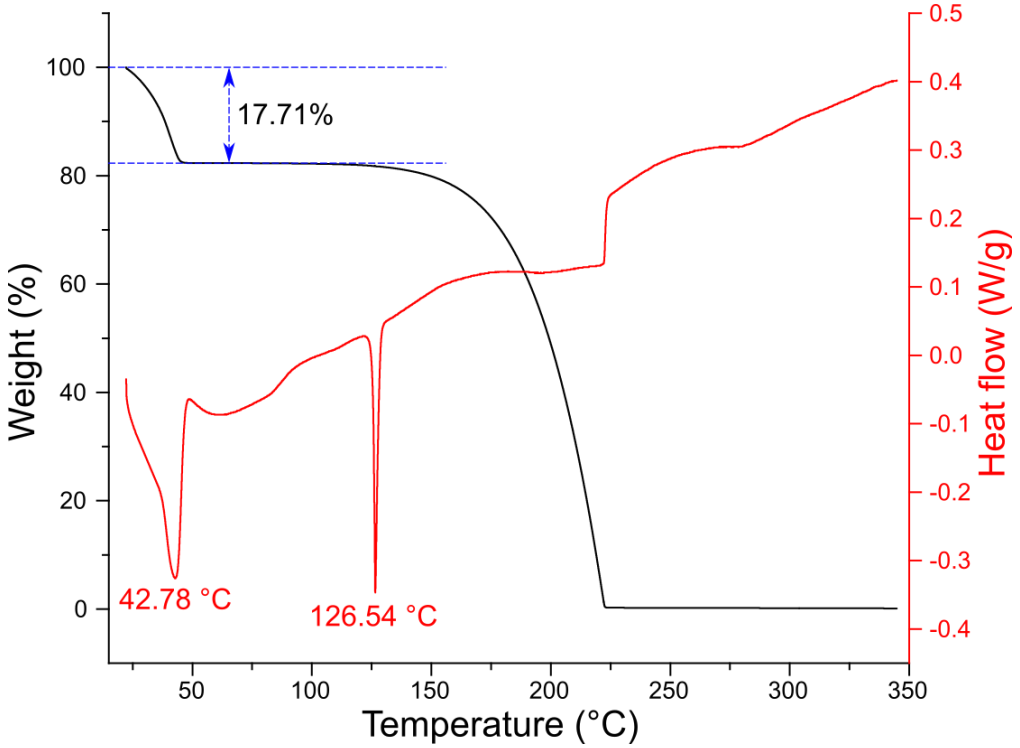

Figure S19. Simultaneous DSC-TGA thermogram for **caf·pyg**·4H_2O cocrystal hydrate.

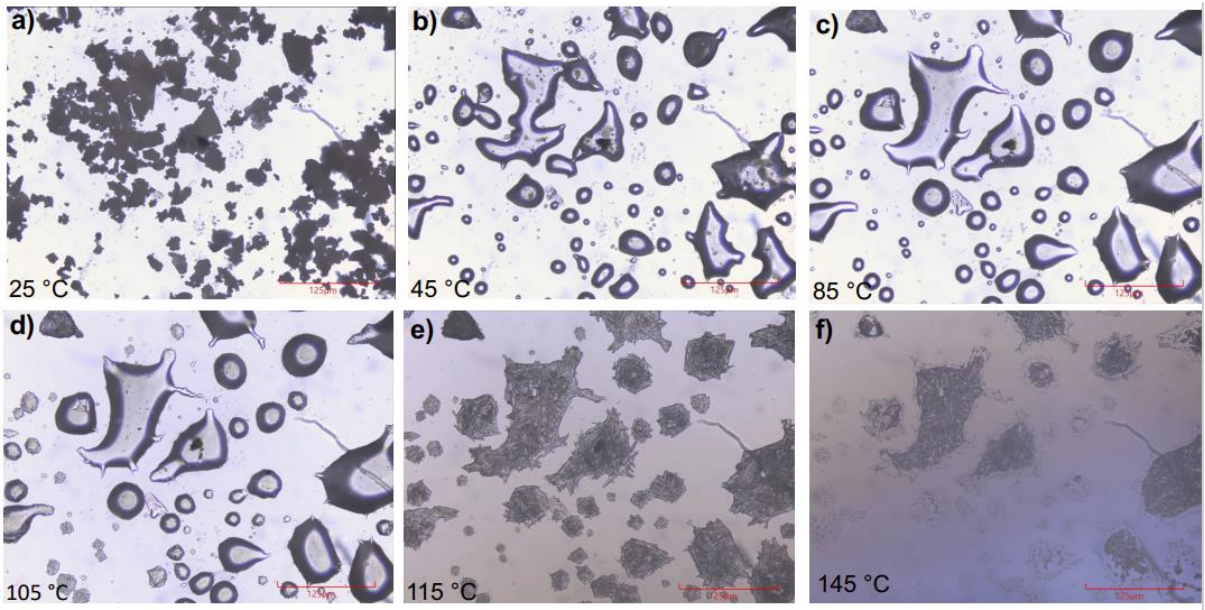

Figure S20. Selected images from a real-time video for a sample of **caf·pyg**·4H_2O, heated at a rate of 1 °C/min in air. Full video is provided as Supplementary Video S1.

S2.6 FTIR-ATR Spectroscopy

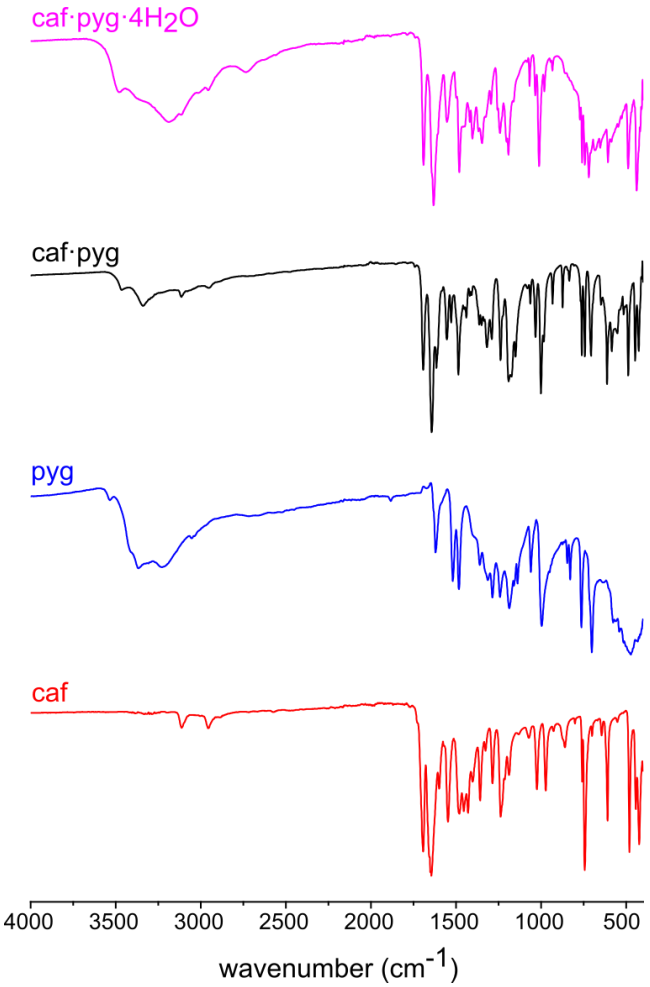

Figure S21. Comparison of FTIR-ATR spectra for (top to bottom): **caf·pyg**·4H_2O, **caf·pyg**, **pyg**, and **caf**.

S2.7 Crystallographic information for caf·pyg·4H$_2$O and caf·pyg

Compound	**caf·pyg**·4H$_2$O	**caf·pyg**
Formula	$C_{14}H_{24}N_4O_9$	$C_{14}H_{16}N_4O_5$
M_r	392.4	320.3
T / K	120.0(1)	120.0(1)
Crystal system	tetragonal	monoclinic
Space group	$P4_2/n$	$P2_1/n$
a / Å	23.1123(5)	13.8775(12)
b / Å	23.1123(5)	7.5913(4)
c / Å	6.8449(2)	15.0147(12)
β / °	90	116.937(10)
V / Å^3	3656.40(19)	1410.2(2)
Z	8	4
ρ_{calc} (g/cm^3)	1.426	1.509
μ/mm^{-1}	1.029	0.987
F(000)	1664.0	672.0
Crystal size / mm^3	0.43 × 0.1 × 0.06	0.20 × 0.12 × 0.11
λ	CuK_α (λ = 1.54184 Å)	CuK_α (λ = 1.54184 Å)
2θ range for data collection/°	7.65 to 154.622	7.206 to 146.102
Data completeness %	98.4	96.6
Index ranges	$-29 \le h \le 28$, $-24 \le k \le 26$, $-8 \le l \le 8$	$-14 \le h \le 16$, $-9 \le k \le 9$, $-18 \le l \le 18$
Reflections collected	19300	12680
Independent reflections	2998 [R_{int} = 0.0403, R_{sigma} = 0.0309]	2730 [R_{int} = 0.0653, R_{sigma} = 0.0417]
Data/restraints/parameters	3825/2/293	2730/0/223
S	1.057	1.070
Final R indexes [$I \ge 2\sigma_I$]	R_1 = 0.0447, wR_2 = 0.1080	R_1 = 0.0469, wR_2 = 0.1226
Final R indexes [all data]	R_1 = 0.0630, wR_2 = 0.1211	R_1 = 0.0562, wR_2 = 0.1310
Largest diff. peak/hole / e Å^{-3}	0.25/-0.34	0.32/-0.32
CCDC deposition codes	2344174	2344173

References

[1] A. Arnone and R. H. Marchessault "*Structure of the Caffeine—Pyrogallol Complex*" in: *Molecular Association in Biological and Related Systems*, Ed. E. D. Goddard, Advances in Chemistry Series, Vol. 84, ACS (1968), 235-258.

[2] C. F. Macrae, I. Sovago, S. J. Cottrell, P. T. A. Galek, P. McCabe, E. Pidcock, M. Platings, G. P. Shields, J. S. Stevens, M. Towler and P. A. Wood, *J. Appl. Cryst.*, 2020, **53**, 226–235.

[3] A. C. Larson, R. B. Von Dreele, Los Alamos National Laboratory Report 2004, LAUR 86–748.

[4] S. J. Clark, M. D. Segall, C. J. Pickard, P. J. Hasnip, M. I. J. Probert, K. Refson and M. C. Payne, *Z. Kristallogr. Cryst. Mater.*, 2005, **220**, 567–570.

[5] T. Björkman, *Comput. Phys. Commun.*, 2011, **182**, 1183–1186.

[6] J. P. Perdew, K. Burke and M. Ernzerhof, *Phys. Rev. Lett.*, 1996, **77**, 3865–3868.

[7] S. Grimme, J. Antony, S. Ehrlich and H. Krieg, *J. Chem. Phys.*, 2010, **132**, 154104.

[8] H. J. Monkhorst and J. D. Pack, *Phys. Rev. B*, 1976, **13**, 5188–5192.

[9] A. Boultif and D. Louër, *J. Appl. Crystallogr.*, 1991, **24**, 987–993.

[10] W. I. F. David, K. Shankland, J. van de Streek, E. Pidcock, W. D. S. Motherwell and J. C. Cole, *J. Appl. Crystallogr.*, 2006, **39**, 910–915.
[11] E. A. Kabova, J. C. Cole, O. Korb, M. Lopez-Ibanez, A. C. Williams and K. Shankland, *J. Appl. Crystallogr*., 2017, **50**, 1411–1420.
[12] E. A. Kabova, J. C. Cole, O. Korb, A. C. Williams and K. Shankland, *J. Appl. Crystallogr.*, 2017, **50**, 1421–1427.
[13] C. R. Groom, I. J. Bruno, M. P. Lightfoot and S. C. Ward, *Acta Cryst.*, 2016, **B72**, 171–179.
[14] H. Rietveld, *J. Appl. Crystallogr.*, 1969, **2**, 65–71.
[15] G. M. Sheldrick, *Acta Cryst*., 1990, **A46**, 467– 473.
[16] G. M. Sheldrick, *Acta Cryst.*, 2015, **B71**, 3– 8.
[17] A. Arnone "The Crystal Structure of the Caffeine-Pyrogallol Complex", M.Sc. Thesis, State University College of Forestry at Syracuse University (1967)